

Numerical analysis of nodal sets for eigenvalues of Aharonov-Bohm Hamiltonians on the square and application to minimal partitions

V. Bonnaillie-Noël* and B. Helffer†

June 27, 2010

Abstract

This paper is devoted to present numerical simulations and interpret theoretically the results for determining the minimal k -partitions of a domain Ω as considered in [14]. More precisely using the double covering approach introduced by B. Helffer, M. and T. Hoffmann-Ostenhof, M. Owen and further developed for questions of isospectrality by the authors in collaboration with T. Hoffmann-Ostenhof and S. Terracini in [14, 4], we analyze the variation of the eigenvalues of the one pole Aharonov-Bohm Hamiltonian on the square and the nodal picture of the associated eigenfunctions as a function of the pole. This leads us to discover new candidates for minimal k -partitions of the square with a specific topological type and without any symmetric assumption, contrary to our previous works [5, 4]. This illustrates also recent results of B. Noris and S. Terracini, see [20, 21]. This finally supports or disproves conjectures for the minimal 3 and 5-partitions on the square.

1 Introduction

1.1 Minimal partitions

For a given partition \mathcal{D} of an open set Ω by k disjoint open subsets D_i , we consider

$$\Lambda(\mathcal{D}) = \max_{i=1,\dots,k} \lambda(D_i), \quad (1.1)$$

where $\lambda(D_i)$ is the groundstate energy of the Dirichlet Laplacian on D_i . We denote the infimum of Λ over all k -partitions of Ω by

$$\mathfrak{L}_k(\Omega) = \inf_{\mathcal{D} \in \mathcal{D}_k} \Lambda(\mathcal{D}). \quad (1.2)$$

We look for minimal k -partitions, i. e. partitions $\mathcal{D} = (D_1, \dots, D_k)$, such that

$$\mathfrak{L}_k(\Omega) = \Lambda(\mathcal{D}).$$

We recall that these minimal k -partitions, whose existence was proven in [8, 10, 9], share with nodal domains many properties of regularity, except that the number of half-lines

*IRMAR, ENS Cachan Bretagne, Univ. Rennes 1, CNRS, UEB, av. Robert Schuman, F-35170 Bruz, France, Virginie.Bonnaillie@bretagne.ens-cachan.fr

†Laboratoire de Mathématiques, Bat. 425, Univ Paris-Sud and CNRS, F-91405 Orsay Cedex, France, Bernard.Helffer@math.u-psud.fr

meeting (with equal angle) at critical points of their boundary set can be odd [14]. Here by critical points we mean points which are at the intersection of at least three distinct ∂D_i 's. Moreover, it was shown in [14] that, if all these numbers are even, then the k -minimal partition consists indeed of the k -nodal domains of some eigenfunction of the Dirichlet Laplacian in Ω .

In [5], we have combined results of [14] and [15] with efficient numerical computations to exhibit some candidates to be minimal 3-partitions for the square, the disk, \dots . This approach was based on the assumption that the minimal 3-partition should inherit from one of the symmetries of the domain. This permits a reduction to a more standard spectral analysis and consequently can only give symmetric candidates. Using two different symmetries of the square, we get the surprise of finding two candidates \mathcal{D}_1 and \mathcal{D}_2 with $\Lambda(\mathcal{D}_1) = \Lambda(\mathcal{D}_2) (\simeq 66.581)$ and give numerical evidence that the unique critical point for these partitions is at the center of the square. These candidates are represented in Figure 1(a). This leads naturally to questions of isospectrality which were solved using the

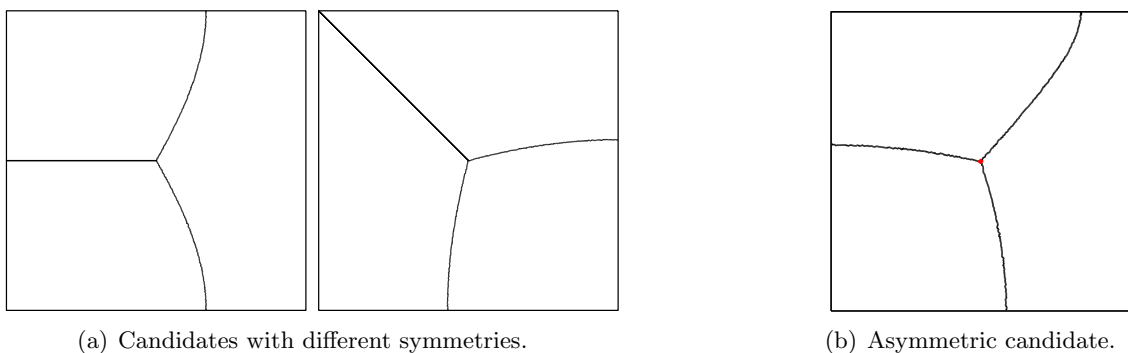


Figure 1: Candidates for the minimal 3-partition of the square.

Aharonov-Bohm Hamiltonian with a singularity at the center of the square, see [4]. This kind of arguments also appears in a similar context in [18] and [17]. Using this operator could provide new asymmetric candidates for the 3-minimal partition (see Figure 1(b)) and it is one of the aims of this paper to exhibit them.

1.2 Aharonov-Bohm Hamiltonian

Let us recall some definitions and results about the Aharonov-Bohm Hamiltonian (for short **ABX**-Hamiltonian) with a singularity at X introduced in [4, 12] and motivated by the work of Berger-Rubinstein [2]. We denote by $X = (x_0, y_0)$ the coordinates of the pole and consider the magnetic potential with renormalized flux $\frac{\Phi}{2\pi} = \frac{1}{2}$ at X :

$$\mathbf{A}^X(x, y) = (A_1^X(x, y), A_2^X(x, y)) = \frac{1}{2} \left(-\frac{y - y_0}{r^2}, \frac{x - x_0}{r^2} \right). \quad (1.3)$$

We know that the magnetic field vanishes identically in $\dot{\Omega}_X$. The **ABX**-Hamiltonian is defined by considering the Friedrichs extension starting from $C_0^\infty(\dot{\Omega}_X)$ and the associated differential operator is

$$-\Delta_{\mathbf{A}^X} := (D_x - A_1^X)^2 + (D_y - A_2^X)^2 \quad \text{with } D_x = -i\partial_x \text{ and } D_y = -i\partial_y. \quad (1.4)$$

Let K_X be the antilinear operator

$$K_X = e^{i\theta_X} \Gamma,$$

with $(x - x_0) + i(y - y_0) = \sqrt{|x - x_0|^2 + |y - y_0|^2} e^{i\theta x}$, and Γ the complex conjugation operator $\Gamma u = \bar{u}$. We say that a function u is K_X -real, if it satisfies $K_X u = u$. Then the operator $-\Delta_{\mathbf{A}x}$ is preserving the K_X -real functions and we can consider a basis of K_X -real eigenfunctions. Hence we only analyze the restriction of the **ABX**-Hamiltonian to the K_X -real space $L^2_{K_X}$ where

$$L^2_{K_X}(\dot{\Omega}_X) = \{u \in L^2(\dot{\Omega}_X), K_X u = u\}.$$

It was shown that the nodal set of such a K_X -real eigenfunction has the same structure as the nodal set of an eigenfunction of the Laplacian except that an odd number of half-lines should meet at X . When no ambiguity exists, we omit sometimes the reference to X and write more simply θ , K , L^2_K , $-\Delta_{\mathbf{A}}$.

1.3 Main goals

Although we will come back to many of these points in the next sections let us comment on some of the difficulties we met in this analysis.

As mentioned previously, we have proposed in [5] some symmetric candidates for the minimal 3-partition. If we do not assume a priori symmetries for a minimal 3-partition, a first method, inspired by [7], is to test the following iterative method (see [6]) :

Initialization. Let $\mathcal{D}_0 = (D_1^0, D_2^0, D_3^0)$ be a 3-partition of Ω .

Iteration. For $n \geq 1$, we define the partition $\mathcal{D}_n = (D_1^n, D_2^n, D_3^n)$ by

- $D_1^n = D_3^{n-1}$,
- (D_2^n, D_3^n) is the nodal partition associated to the second eigenvector of the Dirichlet Laplacian on $\text{Int}(\Omega \setminus D_1^n)$.

If the algorithm converges to the partition $\mathcal{D} = (D_1, D_2, D_3)$, then $\Lambda(\mathcal{D}) = \lambda_1(D_1) = \lambda_1(D_2) = \lambda_1(D_3)$. The results obtained in [6] are at the moment puzzling. Depending on the initial data, on the accuracy and on the form of the domain, all possible situations occur: convergence to the candidate, no convergence, convergence to a non-minimal 3-partition. The case of the equilateral triangle is very strange, the authors get indeed for one of the model a convergence to a three-partition whose energy is clearly above the expected energy, whose singular point is at the center of the symmetry and which is NOT an eigenvalue of the Aharonov-Bohm Hamiltonian. Another method followed by [11] looks also interesting but the paper does not give enough details for permitting an analysis of its efficiency.

In any case, admitting that there exists a perfect good iterative numerical method, it remains interesting on the mathematical level to see that the obtained candidate for a minimal partition is (or is not) a nodal partition for some Hamiltonian. We will come back to this question in the conclusion.

When working on this problem, we realize that we get as a by-product a nice illustration of the general question of analyzing the deformations of the nodal sets and the transition between different nodal structures when varying a parameter. There are actually very few theoretical papers on this question and we also explain the role of the symmetries for solving some questions of avoided crossings or effective crossings, see Section 5.3. This question is very difficult to solve numerically.

We will push a numerical analysis associated with the **ABX**-Hamiltonians with several goals:

- Illustrate the fact that the two symmetric candidates (see Figure 1(a)) for minimal 3-partitions on the square belong actually to a continuous family of non necessarily symmetric candidates (see Figure 1(b) and Figure 8).
- Check, by moving the pole X of the **ABX**-Hamiltonian, the conjecture that the singular point of the minimal 3-partition of the square is at the center.
- Understand and illustrate the mechanism of deformation of the nodal set, and hence extend or guess, in connection with recent papers of B. Noris and S. Terracini [20, 21], some of the properties described in Berger-Rubinstein [2] and Helffer–M.-and-T. Hoffmann-Ostenhof–Owen [12] for the ground state energy (see also [1]).

Finally, let us mention that an extended version of this paper, with more computations, is available in [3]. We have chosen here to focus on the most interesting phenomena.

1.4 Organization of the paper

In Section 2, we explain how we implement the computations on the double covering of the punctured square. In Section 3, we apply Courant’s theorem for comparing the eigenvalues of the Dirichlet Laplacian on the square to the Aharonov-Bohm eigenvalues associated to this puncturing. Section 4 analyzes the dependence of the eigenfunctions of the Dirichlet Laplacian on the double covering with respect to the puncturing point. Section 5 is more specifically devoted to the analysis of the behavior of the nodal sets and eigenvalues when the poles belong respectively to the perpendicular bisector $y = \frac{1}{2}$, the diagonal $y = x$, which correspond to cases when some symmetry of the square is respected in the puncturing. We treat also the case of the axis $y = \frac{1}{4} + \frac{x}{2}$ as an example of a generic situation. Section 6 describes the possible applications of our analysis of nodal sets to the research of minimal partitions with a given topological type. We conclude by the presentation of a conjecture motivated by our computations.

Acknowledgements.

The authors would like to thank Thomas Hoffmann-Ostenhof, Luc Hillairet and Susanna Terracini for useful discussions around this topics. We have been in particular stimulated by successive versions of [20]. Discussions about numerics with François Alouges and Grégory Vial were also very fruitful. G. Vial helps us moreover by realizing numerous meshes for the computations and also for the detection of the nodal lines.

This paper has been partially written during the stay of the authors at the Erwin Schrödinger Institute from May to July 2009 and the authors are grateful for the very good working conditions and also for the fruitful discussions with other participants of the workshop on Topics in Spectral Theory.

2 Numerical implementation

The **ABX**-Hamiltonian has a singularity at the pole X and the eigenfunctions are complex-valued. For these reasons, we prefer to deal with the Dirichlet Laplacian on the double-covering $\dot{\Omega}_X^{\mathcal{R}}$ whose eigenfunctions are real-valued. Some of these eigenfunctions, which will be described below, are directly related with the K_X -real eigenfunctions of the **ABX**-Hamiltonian, as mentioned in [4, Section 6.3]. For the construction of the double covering, we choose a simple line γ_X joining the pole to the boundary such that $\Omega \setminus \gamma_X$ is simply connected. This path permits to go from one sheet to the other one.

The numerical results were realized by using the Finite Element Library MÉLINA (see [19]). The method is completely standard but the new idea is to work on the double covering of a pointed domain. The computations consist only of the determination of the eigenfunctions of a Dirichlet Laplacian on a double covering domain. Nevertheless, since we are interested in the nodal lines of these eigenfunctions, computations have to be quite accurate and we choose the package MÉLINA permitting the implementation of high order elements.

The main point of the numerical part consists in meshing the double covering $\dot{\Omega}_X^{\mathcal{R}}$ of the punctured domain $\Omega \setminus \{X\}$. To do this, we use the two-dimensional mesh generator TRIANGLE (see [22]). Let us explain in more details how we proceed.

Let Ω be the square $[0, 1] \times [0, 1]$ and X be a point in $[0, \frac{1}{2}] \times [0, \frac{1}{2}]$. We start with meshing the domain Ω so that (see Fig. 2):

- the segment joining $(0, 0)$ to the pole X , in red in Figure 2, does not go through any element of the mesh,
- the segment $[(0, 0); X]$ is the union of edges of an even number of triangles,
- the pole X is the vertex of some triangles.

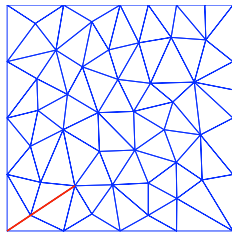


Figure 2: Mesh of the double covering $\dot{\Omega}_X^{\mathcal{R}}$.

This first mesh is essentially done for the first sheet and we repeat this mesh for the second sheet. To obtain a mesh of the double covering $\dot{\Omega}_X^{\mathcal{R}}$, we choose as a cutting line the segment $\gamma_X = [(0, 0); X]$ and we have to exchange the vertex along the segment $[(0, 0); X]$ between the first and second sheet. Then we remove the point X of the second sheet by equaling it to the vertex X of the first sheet. For the numerics, X will be chosen on the lattice $\mathcal{P} = \{(\frac{i}{100}, \frac{j}{100}), 1 \leq i, j \leq 50\}$.

Theoretically, the eigenvalues and eigenfunctions depend only on the pole and are independent of the cut chosen for our construction. The introduction of the segment $[(0, 0); X]$ is only a technical point and we have verified that the numerical computations of the eigenfunctions and eigenvalues are (with a rather good accuracy $\sim 10^{-3}$) independent of the choice of the line joining the pole to the boundary, that is the line between the first and second sheet. Many computations corresponding to two different choices of cutting lines are available on the web page (see [6]):

<http://w3.bretagne.ens-cachan.fr/math/simulations/MinimalPartitions/covering.php>
The computed eigenvalues are given all along this paper with an approximation at $5 \cdot 10^{-4}$.

In the following, we use a \mathbb{P}^6 approximation with at least 6000 elements. To detect the nodal lines, we use a program realized by G. Vial. The idea is that it is very easy to compute the zero set of linear functions. In our case, we deal with a function which is piecewise \mathbb{P}^k and given by a finite element method. We know the values of this function at some points. As soon as we have these values, we can replace this function by a

new function which is piecewise linear. For this, we introduce some new points by an interpolation method. Then we detect the zero set of this new function.

3 A few theoretical comparison theorems

3.1 Notation

We denote by Ω the square $[0, 1] \times [0, 1]$ and by $C = (\frac{1}{2}, \frac{1}{2})$ the center of the square. We compute the eigenfunctions of the Laplacian on the double covering $\dot{\Omega}_X^{\mathcal{R}}$ of $\dot{\Omega}_X = \Omega \setminus \{X\}$. By a symmetry argument, it is enough to consider $X = (x_0, y_0)$ in the quarter square $[0, \frac{1}{2}] \times [0, \frac{1}{2}]$.

There are two ways of labelling the eigenvalues.

We can label it in the standard way and then denote by $\lambda_k(\dot{\Omega}_X^{\mathcal{R}})$ the k -th eigenvalue of the Dirichlet Laplacian on $\dot{\Omega}_X^{\mathcal{R}}$.

We can also take account of the symmetry relative to the deck map $\mathcal{D}_X^{\mathcal{R}}$ associating with a given point in the covering the distinct point with same projection by the covering map $\pi_X^{\mathcal{R}}$ of $\dot{\Omega}_X^{\mathcal{R}}$ onto $\dot{\Omega}_X$. This splits the spectrum into two independent spectra relative to two orthogonal spaces in $L^2(\dot{\Omega}_X^{\mathcal{R}})$.

The eigenvalues correspond

- either to eigenfunctions lifted from the eigenfunctions (of the Dirichlet Laplacian)¹ on the square by the covering map (sometimes called $\mathcal{D}_X^{\mathcal{R}}$ -symmetric because they are symmetric with respect to the deck map),
- or to eigenfunctions which are $\mathcal{D}_X^{\mathcal{R}}$ -antisymmetric with respect to the deck map. We also call them **ABX**-eigenvalues because they can be seen as eigenvalues of an **AB**-Hamiltonian with a pole X creating a renormalized flux equal to $\frac{1}{2}$. We shortly write **ABX**-Hamiltonian if we want to make explicit the reference to the pole. We denote by $\lambda_j^{\mathbf{ABX}} = \lambda_j^{\mathbf{AB}}(\dot{\Omega}_X)$ the j -th eigenvalue of the **AB**-Hamiltonian with pole at X .

In consequence, for any pole X and any integer k , the eigenvalue $\lambda_k(\dot{\Omega}_X^{\mathcal{R}})$ of the Dirichlet Laplacian on the double covering is either an eigenvalue $\lambda_j(\Omega)$ of the square, either an eigenvalue $\lambda_j^{\mathbf{ABX}}$ of the **AB**-Hamiltonian on $\dot{\Omega}_X$ with pole at X .

3.2 Eigenvalues of the square

The eigenvalues of the square are well known and given by the double sequence $\pi^2(m^2+n^2)$ with $m \in \mathbb{N} \setminus \{0\}, n \in \mathbb{N} \setminus \{0\}$, with corresponding basis of eigenfunctions given by

$$\Omega \ni (x, y) \mapsto \phi_{mn}(x, y) := \sin(m\pi x) \sin(n\pi y).$$

Labelling the eigenvalues in increasing order leads to the sequence denoted by $\lambda_k(\Omega)$, $k \in \mathbb{N}^*$. Table 1 gives the first eight eigenvalues and the nodal set of the associated eigenfunctions belonging to the above basis. The second, fifth and seventh eigenvalues are double and consequently, it is also natural to look at the nodal sets of linear combinations in order to determine all the possible nodal configurations associated with this eigenvalue.

We notice that the $\mathcal{D}_X^{\mathcal{R}}$ -symmetric spectrum of the Dirichlet Laplacian on the double covering $\dot{\Omega}_X^{\mathcal{R}}$ is the spectrum of the square and is independent of the pole. This is a consequence of the fact that the spectra of the Dirichlet Laplacian in Ω and $\dot{\Omega}_X$ are the

¹We sometimes speak more shortly of spectrum of the square.

Eigenvalues of the square	(m, n) -labelling	Nodal sets for ϕ_{mn}
$\lambda_1(\Omega) = 2\pi^2 \simeq 19.739$	(1, 1)	
$\lambda_2(\Omega) = \lambda_3(\Omega) = 5\pi^2 \simeq 49.348$	(2, 1) , (1, 2)	
$\lambda_4(\Omega) = 8\pi^2 \simeq 78.957$	(2, 2)	
$\lambda_5(\Omega) = \lambda_6(\Omega) = 10\pi^2 \simeq 98.696$	(3, 1) , (1, 3)	
$\lambda_7(\Omega) = \lambda_8(\Omega) = 13\pi^2 \simeq 128.305$	(3, 2) , (2, 3)	

Table 1: First eight eigenvalues of the Dirichlet Laplacian on Ω and nodal sets for the associated basis ϕ_{mn} .

same, the puncturing point being of capacity 0. So it is more the **ABX**-spectrum which is of interest because depending on the position of the pole. Nevertheless, the standard labelling of all the eigenvalues on $\dot{\Omega}_X^{\mathcal{R}}$ can play a role when applying Courant's theorem. Of course we have $\lambda_1(\dot{\Omega}_X^{\mathcal{R}}) = \lambda_1(\Omega)$.

3.3 Theoretical estimates of the eigenvalues

This subsection is concerned with the comparison between the spectrum on the square, the spectrum on the double covering $\dot{\Omega}_X^{\mathcal{R}}$ and the **ABX**-spectrum. We propose some equalities and upper bounds between the eigenvalues essentially based on the minimax principle and on the Courant's nodal theorem which is recalled now.

Theorem 3.1

Let $k \geq 1$, $\lambda_k(D)$ be the k -th eigenvalue for the Dirichlet Laplacian on D . Then any associated eigenfunction has at most k nodal domains.

We would also apply this theorem for the K_X -real eigenfunctions of the **ABX**-Hamiltonian on $\dot{\Omega}_X$. Equivalently, this corresponds to a Courant nodal theorem for the $\mathcal{D}_X^{\mathcal{R}}$ -antisymmetric eigenfunctions on $\dot{\Omega}_X^{\mathcal{R}}$, already discussed in [4]. Combination of the Courant nodal theorem and Max-Min principle for the **ABX**-Hamiltonian leads to the following proposition.

Proposition 3.2

Let $X \in [0, \frac{1}{2}] \times [0, \frac{1}{2}]$, then

$$\lambda_1(\Omega) = \lambda_1(\dot{\Omega}_X^{\mathcal{R}}), \quad \lambda_1^{\mathbf{ABX}} = \lambda_2(\dot{\Omega}_X^{\mathcal{R}}), \quad \lambda_2^{\mathbf{ABX}} = \lambda_3(\dot{\Omega}_X^{\mathcal{R}}), \quad (3.1)$$

and for $k = 2, 4, 5, 7, 9, 11$, there exists an integer ℓ_k such that

$$\lambda_2^{\mathbf{ABX}} < \lambda_2(\Omega) = \lambda_{\ell_2}(\dot{\Omega}_X^{\mathcal{R}}) \text{ with } \ell_2 \geq 4 \text{ (with multiplicity at least 2)}, \quad (3.2)$$

$$\lambda_3^{\mathbf{ABX}} \leq \lambda_4(\Omega) = \lambda_{\ell_4}(\dot{\Omega}_X^{\mathcal{R}}) \text{ with } \ell_4 \geq 7, \quad (3.3)$$

$$\lambda_5(\Omega) = \lambda_{\ell_5}(\dot{\Omega}_X^{\mathcal{R}}) \text{ with } \ell_5 \geq 8, \quad (3.4)$$

$$\lambda_5^{\mathbf{ABX}} \leq \lambda_7(\Omega) = \lambda_{\ell_7}(\dot{\Omega}_X^{\mathcal{R}}) \text{ with } \ell_7 \geq 12, \quad (3.5)$$

$$\lambda_9(\Omega) = \lambda_{\ell_9}(\dot{\Omega}_X^{\mathcal{R}}) \text{ with } \ell_9 \geq 14, \quad (3.6)$$

$$\lambda_8^{\mathbf{ABX}} \leq \lambda_{11}(\Omega) = \lambda_{\ell_{11}}(\dot{\Omega}_X^{\mathcal{R}}) \text{ with } \ell_{11} \geq 19. \quad (3.7)$$

If X belongs to the perpendicular bisectors of the square, we have more accurately:

$$\ell_4 = \ell_4(X) \geq 8, \quad (3.8)$$

$$\lambda_6^{\mathbf{ABX}} \leq \lambda_7(\Omega). \quad (3.9)$$

Remark 3.3

The multiplicity of $\lambda_\ell(\Omega)$ as eigenvalue of the Dirichlet Laplacian on $\dot{\Omega}_X^{\mathcal{R}}$ is of course larger or equal to its multiplicity on Ω . This could permit to improve some inequalities above when we can find for a given pole an eigenfunction u of the Dirichlet Laplacian on Ω vanishing at the pole. The number of nodal domains of the lifted symmetric function on the covering is then $2\mu(u)$ instead of $2\mu(u) - 1$ where $\mu(u)$ is the number of nodal domains of u . To find this eigenfunction could be easier when the eigenspace is of higher dimension. This appears for example for $\lambda_2(\Omega)$.

Proof : Let us first prove (3.2). We first observe that, for any $X \in [0, \frac{1}{2}] \times [0, \frac{1}{2}]$, there exists an eigenfunction u_X of the Dirichlet Laplacian associated with $\lambda_2(\Omega)$ and $u_X(X) = 0$. We have just to look for u_X of the form $u_X = \alpha\phi_{1,2} + \beta\phi_{2,1}$ with $(\alpha, \beta) \neq (0, 0)$ satisfying $\alpha\phi_{1,2}(X) + \beta\phi_{2,1}(X) = 0$. By lifting on $\dot{\Omega}_X^{\mathcal{R}}$, this gives a $\mathcal{D}_X^{\mathcal{R}}$ -symmetric eigenfunction $u_X \circ \pi_X^{\mathcal{R}}$ for the Dirichlet Laplacian on $\dot{\Omega}_X^{\mathcal{R}}$ with four nodal domains and associated with $\lambda_2(\Omega)$. Hence by Courant's theorem, $\lambda_2(\Omega) = \lambda_{\ell_2}(\dot{\Omega}_X^{\mathcal{R}})$ with $\ell_2 \geq 4$. To establish the first inequality in (3.2), we consider the functions $\max(u_X, 0)$ and $\max(-u_X, 0)$, which span a two-dimensional space in the form domain of the \mathbf{ABX} -Hamiltonian for which the energy is less than $\lambda_2(\Omega)$. We can conclude by the minimax principle. It is easy to see that the inequality is strict. Hence at this stage we also get (3.2).

Let us now prove (3.3). Using the three functions obtained by restriction to one nodal domain of the function $\phi_{2,2}$ (then extended by 0) which does not contain X , we obtain a 3-dimensional space of functions in the form domain of the \mathbf{ABX} -Hamiltonian for which the energy is less than $\lambda_4(\Omega)$ (or a 4-dimension space if X is on the perpendicular bisector to the side of the square because we can in this case get a 4-dimensional space, see Remark 3.3). We then conclude by the minimax principle. The relation with $\lambda_{\ell_4}(\dot{\Omega}_X^{\mathcal{R}})$ is an application of the Courant's nodal theorem using the function $\phi_{2,2} \circ \pi_X^{\mathcal{R}}$.

Relation (3.4) is a consequence of (3.3).

For (3.5), we can this time use the function $\phi_{3,2}$ which has at least 5 nodal domains not containing X . For X on the perpendicular bisector, we get (3.9).

The function $\phi_{4,1}$ has at least 3 nodal domains not containing X . Using (3.5) and the multiplicity of $\lambda_9(\Omega)$, we obtain (3.6).

Using the function $\phi_{3,3}$ which has at least 8 nodal domains not containing X , we deduce (3.7).

The lower bound for ℓ_7, ℓ_9 and ℓ_{11} results immediately of the upper bounds of $\lambda_5^{\mathbf{ABX}}$ by $\lambda_7(\Omega)$ (hence by $\lambda_9(\Omega)$) and of $\lambda_8^{\mathbf{ABX}}$ by $\lambda_{11}(\Omega)$ established in (3.5) and (3.7). \square

Lemma 3.4

The nodal set of the second K_X -real eigenfunction $u_2^{\mathbf{ABX}}$ consists of one line joining the pole X to the boundary.

Proof :

We know from [12] that a piecewise regular line in the nodal set should join the pole X to the boundary. Another piece in the nodal set should necessary create an additional nodal domain which will lead to $\lambda_2 \leq \lambda_2^{\mathbf{ABX}}$ in contradiction to (3.2). \square

The inequality $\lambda_1^{\mathbf{ABX}} \geq \lambda_1(\Omega)$ is of course a particular case of the diamagnetic inequality. We will observe on the pictures that the situation is much more complicate for the excited states. Except in the case of additional symmetries where some monotonicity will be proven, we have no theoretical results.

Remark 3.5

We will see in Figures 11, 12 and 16, that the upper bounds (3.2), (3.3) and (3.5) in Proposition 3.2 for the \mathbf{ABX} -eigenvalues are optimal in the sense that we can find a pole such that the upper bound is false with a smaller eigenvalue of the square.

4 Behavior of the eigenvalues on the double covering of the punctured square, when moving the pole

In this section, we start to discuss the influence of the location of the puncturing point X (or pole) on the topological structure of the nodal set of the first eigenfunctions.

4.1 Behavior when the pole tends to the boundary

It has been announced by B. Noris and S. Terracini [20, 21] that the k -th \mathbf{ABX} -eigenvalue of the punctured square tends to the k -th eigenvalue of the Dirichlet Laplacian on the square as the pole tends to the boundary (see also [16] for connected results). They also establish in [20] the continuity with respect to a pole and prove that $X \mapsto \lambda_k^{\mathbf{ABX}}$ is of class C^1 if $\lambda_k^{\mathbf{ABX}}$ is simple. Because after a translation by X , we get a fixed operator with moving regular boundary and fixed pole at $(0, 0)$, the regularity is actually easy. These results are illustrated in Figures 3–7 which represent the eigenvalues $\lambda_k(\dot{\Omega}_X^{\mathcal{R}})$, $k = 2, 3, 6, 7$, according to the location of the pole $X \in \mathcal{P}$ and Table 2 which gives the first 12 eigenvalues of the Dirichlet Laplacian on $\dot{\Omega}_X^{\mathcal{R}}$ for three points X : one near the boundary denoted by A , one at the center denoted by C and one other denoted by B .

n	$\lambda_n(\dot{\Omega}_A^{\mathcal{R}})$	$\lambda_n(\dot{\Omega}_B^{\mathcal{R}})$	$\lambda_n(\dot{\Omega}_C^{\mathcal{R}})$
1	19.739	19.739	19.739
2	19.739	20.269	33.528
3	49.348	49.325	33.534
4	49.348	49.348	49.348
5	49.348	49.348	49.348
6	49.348	51.480	66.581
7	78.957	78.957	66.581
8	78.957	79.536	78.957
9	98.696	98.658	98.696
10	98.696	98.696	98.696
11	98.696	98.696	111.910
12	98.696	102.647	111.910

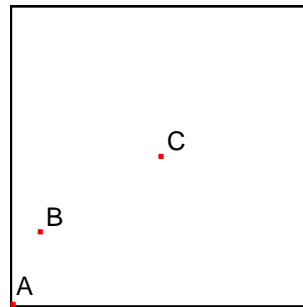


Table 2: First 12 eigenvalues of the Dirichlet Laplacian on $\dot{\Omega}_A^{\mathcal{R}}$, $\dot{\Omega}_B^{\mathcal{R}}$ and $\dot{\Omega}_C^{\mathcal{R}}$, with $A = (\frac{1}{100}, \frac{1}{100})$, $B = (\frac{1}{10}, \frac{2}{5})$, $C = (\frac{1}{2}, \frac{1}{2})$.

4.2 Eigenvalues 2 to 5

We observe numerically, see Figure 3, that for $X \in \mathcal{P}$, the function $X \mapsto \lambda_2(\dot{\Omega}_X^{\mathcal{R}})$ has a global maximum, denoted by λ_2^{max} for $X = C$ and is minimal when X belongs to the boundary $x = 0$ or $y = 0$. This minimum equals $\lambda_2(\Omega)$. Moreover we do not observe other critical points in \mathcal{P} . Looking at Figure 4, we observe numerically that the function $X \mapsto \lambda_3(\dot{\Omega}_X^{\mathcal{R}})$ behaves conversely: it has a global minimum, denoted by λ_3^{min} , for $X = C$

and the maximum is reached at the boundary $x = 0$ or $y = 0$ and equals $\lambda_3(\Omega)$. We have monotonicity along lines joining a point of the boundary to the center C . Furthermore, we notice that $\lambda_2^{max} = \lambda_3^{min}$.

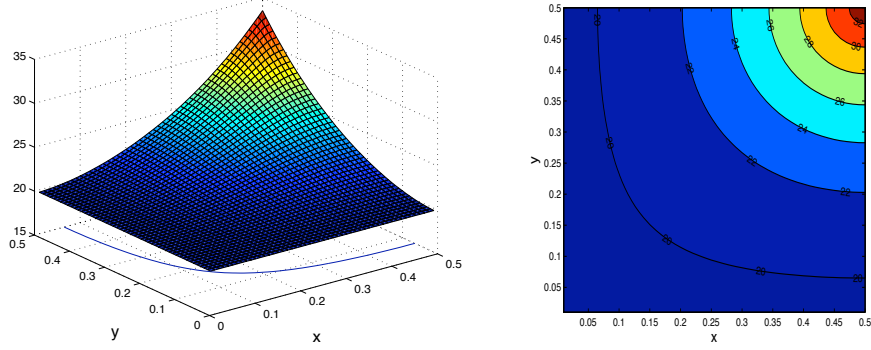


Figure 3: $X \mapsto \lambda_2(\dot{\Omega}_X^{\mathcal{R}})$ for $X \in \mathcal{P}$.

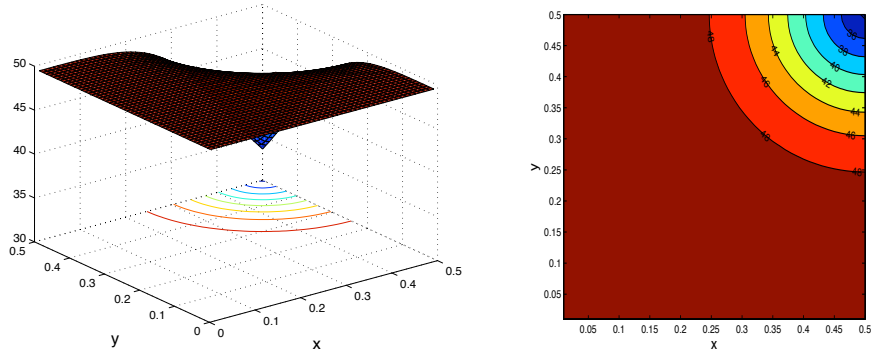


Figure 4: $X \mapsto \lambda_3(\dot{\Omega}_X^{\mathcal{R}})$ for $X \in \mathcal{P}$.

Figure 5 gives the eigenvalues and the nodal lines of the eigenfunctions associated with the second and third eigenvalues of the Dirichlet Laplacian on $\dot{\Omega}_X^{\mathcal{R}}$ on the first and second lines respectively. The j -th column corresponds to the domain $\dot{\Omega}_{X_j}^{\mathcal{R}}$ with $X_j = (\frac{1}{5}, \frac{j}{10})$, $j = 1, \dots, 5$. These figures are illustration of the theory of Berger–Rubinstein [2] and Helffer–Hoffmann–Ostenhof–Hoffmann–Ostenhof–Owen [12] (see also [1]). For the ground state energy, we recover the theorem of these authors that the nodal set is composed of a line joining the pole to the boundary. We observe that the nodal line in the first case is choosing a kind of minimal distance between the pole and the boundary whereas the nodal line in the second case seems to choose a kind of maximal distance. We do not have a rigorous explanation for this property except that it should be related to the theorem proved in [2, 12] that $\lambda_1^{\mathbf{AB}X}$ is the infimum over the Dirichlet eigenvalue of the Laplacian in $\Omega \setminus \gamma$ where γ is a regular path joining the pole X to the boundary.

We also recover the two last equations in (3.1).

Using (3.2), we have proved that $\lambda_2(\Omega) \geq \lambda_5(\dot{\Omega}_X^{\mathcal{R}})$. We observe numerically (see also ahead Figures 11 and 12 for poles along a symmetry axis and Figure 16) that, for any $X \in \mathcal{P}$, we have

$$\lambda_4(\dot{\Omega}_X^{\mathcal{R}}) = \lambda_5(\dot{\Omega}_X^{\mathcal{R}}) = \lambda_2(\Omega). \quad (4.1)$$

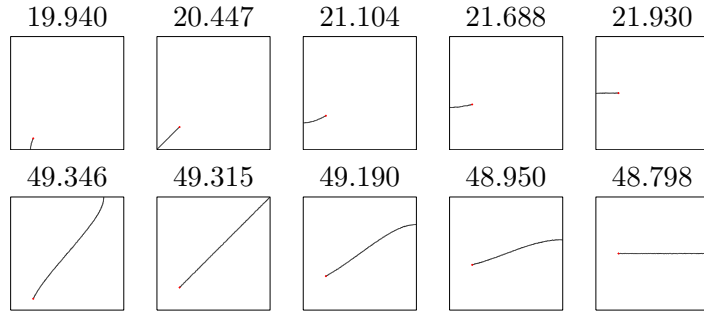


Figure 5: Nodal set for the eigenfunctions associated with $\lambda_k(\dot{\Omega}_X^{\mathcal{R}})$, $k = 2, 3$, for poles $X = (\frac{1}{5}, \frac{j}{10})$, $1 \leq j \leq 5$.

4.3 Eigenvalues 6 and 7

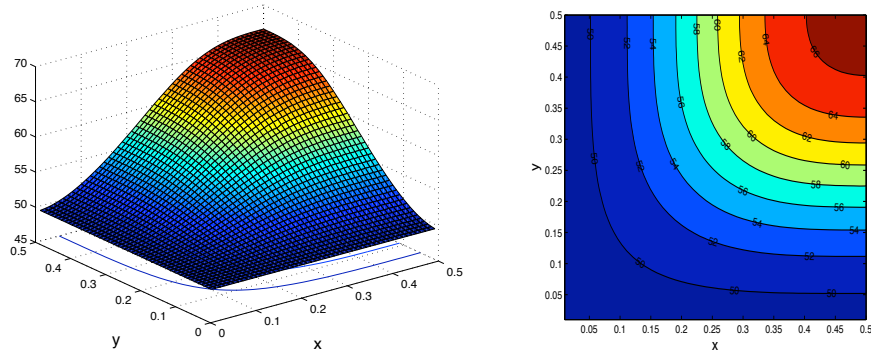


Figure 6: $\lambda_6(\dot{\Omega}_X^{\mathcal{R}})$, in function of the pole $X \in \mathcal{P}$.

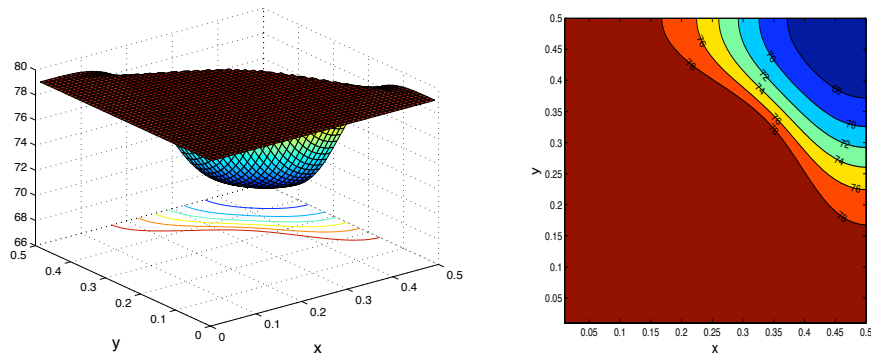


Figure 7: $\lambda_7(\dot{\Omega}_X^{\mathcal{R}})$, in function of the pole $X \in \mathcal{P}$.

Numerics shows that the 6-th eigenvalue $\lambda_6(\dot{\Omega}_X^{\mathcal{R}})$ is minimal at the boundary and has a unique maximum $\lambda_6^{max} \simeq 66.581$ reached for the pole at the center. We do not observe other critical points. The 7-th eigenvalue $\lambda_7(\dot{\Omega}_X^{\mathcal{R}})$ is minimal when the pole is at the center and its minimum λ_7^{min} is equal to λ_6^{max} . When the pole is at the center, the zero set of the 6-th eigenfunction provides, by projection, a candidate for a 3-partition and λ_6^{max} is the conjectured value for $\mathcal{L}_3(\Omega)$. We observe that the 7-th eigenvalue becomes constant equal

to $\lambda_7^{max} = \lambda_4(\Omega) = 8\pi^2$ as a function of the pole when the pole is close to the boundary. This corresponds to a crossing when X approaches the boundary between the spectrum of the square (i.e. the $\mathcal{D}_X^{\mathcal{R}}$ -symmetric spectrum on the covering) and the X -dependent **ABX**-spectrum (i.e. the $\mathcal{D}_X^{\mathcal{R}}$ -antisymmetric spectrum on the covering $\dot{\Omega}_X^{\mathcal{R}}$). Applying relation (3.3), we have proved theoretically that $\lambda_4(\Omega) \geq \lambda_7(\dot{\Omega}_X^{\mathcal{R}})$. We observe numerically that this relation is optimal in the sense that we have equality for X close to the boundary.

Considering the linear combination of the eigenfunctions u_6 and u_7 associated respectively with $\lambda_6(\dot{\Omega}_C^{\mathcal{R}})$ and $\lambda_7(\dot{\Omega}_C^{\mathcal{R}})$, with $C = (\frac{1}{2}, \frac{1}{2})$, we can construct a family of 3-partitions with the same energy. Figure 8 gives the projection by $\pi_C^{\mathcal{R}}$ of the nodal set for the functions $tu_6 + (1-t)u_7$ with $t = k/8$, $k = 0, \dots, 8$.

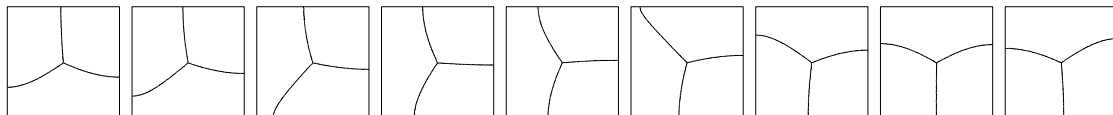


Figure 8: Continuous family of 3-partitions with the same energy.

It is interesting to discuss if we can prove the numerically observed inequality

$$\lambda_3^{\mathbf{ABX}} \geq \lambda_2(\Omega). \quad (4.2)$$

This is directly related to the conjecture proposed by S. Terracini²:

Conjecture 4.1

Except at the center $X = C = (\frac{1}{2}, \frac{1}{2})$, $\lambda_3^{\mathbf{ABX}}$ is simple and the corresponding nodal set of the K_X -real eigenfunction is the union of a line joining the pole to the boundary and of another line joining two points of the boundary.

We note indeed that if the conjecture is true, we will get (4.2) by the minimax principle.

4.4 Eigenvalues 8 to 10

Figures 9–10 represent the numerical computations of $\lambda_8(\dot{\Omega}_X^{\mathcal{R}})$ and $\lambda_9(\dot{\Omega}_X^{\mathcal{R}})$ for $X \in \mathcal{P}$. We observe numerically that the function $X \mapsto \lambda_8(\dot{\Omega}_X^{\mathcal{R}})$ has a unique maximum denoted by λ_8^{max} at a point C_1 on the diagonal and $X \mapsto \lambda_9(\dot{\Omega}_X^{\mathcal{R}})$ reaches its unique minimum, λ_9^{min} , at this point. We can recover this behavior on Figure 11 where are drawn the eigenvalues for poles on the diagonal. Numerically, $\lambda_8^{max} = \lambda_9^{min}$ and we come back to this equality in Subsection 5 where we look at the nodal lines of the eigenfunctions associated with $\lambda_8(\dot{\Omega}_X^{\mathcal{R}})$ and $\lambda_9(\dot{\Omega}_X^{\mathcal{R}})$ and predict the existence of the point C_1 , see Figure 14(a).

According to (3.8), we have proved that $\lambda_8(\dot{\Omega}_X^{\mathcal{R}}) \leq \lambda_7(\Omega)$. This theoretical upper bound is rough and the numerics suggests that we have in fact the better bound $\lambda_8(\dot{\Omega}_X^{\mathcal{R}}) \leq \lambda_5(\Omega)$. Moreover C_1 is singular for the maps $X \mapsto \lambda_8(\dot{\Omega}_X^{\mathcal{R}})$ and $\lambda_9(\dot{\Omega}_X^{\mathcal{R}})$.

We observe numerically that, for any $X \in \mathcal{P}$, we have

$$\lambda_{10}(\dot{\Omega}_X^{\mathcal{R}}) = \lambda_5(\Omega). \quad (4.3)$$

What we have proven in (3.4) is weaker.

²Personal communication

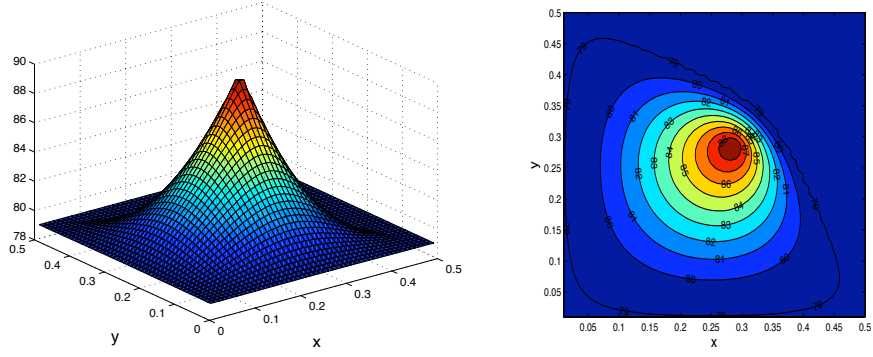


Figure 9: $X \mapsto \lambda_8(\dot{\Omega}_X^{\mathcal{R}})$ for $X \in \mathcal{P}$.

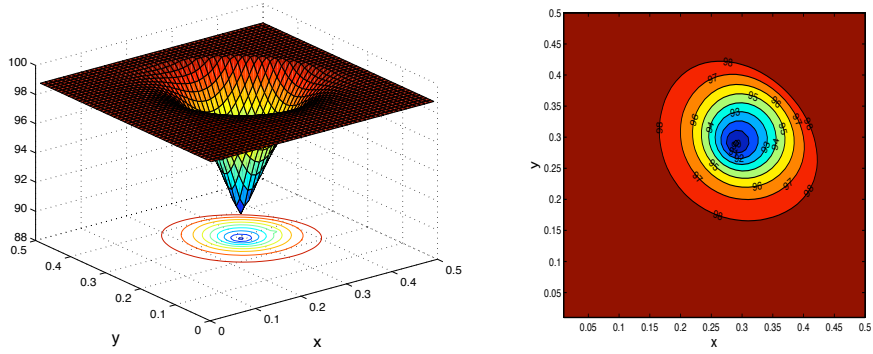


Figure 10: $X \mapsto \lambda_9(\dot{\Omega}_X^{\mathcal{R}})$ for $X \in \mathcal{P}$.

5 Moving the pole along symmetry axis

5.1 Analysis of the symmetries

Let us begin with some considerations about the **ABX**-Hamiltonian on the X -punctured square, using the symmetry along the perpendicular bisector $y = \frac{1}{2}$ or the diagonal $y = x$. We refer to [4] for more details. The square is invariant under the symmetries

$$\sigma_1(x, y) = (x, 1 - y) \quad \text{and} \quad \sigma_2(x, y) = (y, x).$$

We consider the antilinear operators

$$\Sigma_j^c = \Gamma \Sigma_j, \quad j = 1, 2,$$

where Γ is the complex conjugation ($\Gamma u = \bar{u}$) and Σ_j is associated with σ_j by the relation $\Sigma_1 u(x, y) = u(x, 1 - y)$ and $\Sigma_2 u(x, y) = u(y, x)$.

We use the symmetry of the X -punctured square to give an orthogonal decomposition of $L_K^2 = L_{K_X}^2$:

$$L_K^2 = L_{K, \Sigma_j}^2 \oplus L_{K, a \Sigma_j}^2, \quad (5.1)$$

where

$$L_{K, \Sigma_j}^2 = \{u \in L_K^2, \Sigma_j^c u = u\}, \quad \text{and} \quad L_{K, a \Sigma_j}^2 = \{u \in L_K^2, \Sigma_j^c u = -u\}. \quad (5.2)$$

As established in [4, Lemma 5.6], we can prove that:

if $X = (x_0, \frac{1}{2})$:

- if $u \in C^\infty(\dot{\Omega}_X) \cap L^2_{K, \Sigma_1}$, then its nodal set contains $[0, x_0] \times \{\frac{1}{2}\}$,
- if $u \in C^\infty(\dot{\Omega}_X) \cap L^2_{K, a\Sigma_1}$, then its nodal set contains $[x_0, 1] \times \{\frac{1}{2}\}$,

if $X = (x_0, x_0)$:

- if $u \in C^\infty(\dot{\Omega}_X) \cap L^2_{K, \Sigma_2}$, then the nodal set of u contains $\{(x, x), 0 < x < x_0\}$,
- if $u \in C^\infty(\dot{\Omega}_X) \cap L^2_{K, a\Sigma_2}$, then the nodal set of u contains $\{(x, x), x_0 < x < 1\}$.

Dealing with a mixed Dirichlet-Neumann condition on the half-domain, we deduce that the eigenvalues for which the eigenfunctions are symmetric are increasing with respect to x_0 , whereas the eigenvalues for which the eigenfunctions are antisymmetric are decreasing with respect to x_0 .

5.2 Spectral variation

Figures 11 and 12 give the eigenvalues for poles along the axis $y = \frac{1}{2}$ and $y = x$ respectively and $0 < x \leq \frac{1}{2}$. Poles are denoted by $X(x) = (x, \frac{1}{2})$ and $\check{X}(x) = (x, x)$. The below mentioned symmetry (resp. antisymmetry) is in this section with respect to Σ_j^c (see (5.2)) and denoted by Σ_j (resp. $a\Sigma_j$) on the figures where $j = 1$ when we consider poles $X(x)$ and $j = 2$ for poles $\check{X}(x)$.

Let us first mention some numerical observations available for these two configurations:

- $\lim_{x \rightarrow 0} \lambda_k^{\mathbf{AB}X(x)} = \lambda_k(\Omega)$ and $\lim_{x \rightarrow 0} \lambda_k^{\mathbf{AB}\check{X}(x)} = \lambda_k(\Omega)$.
- For any integer $0 \leq k \leq 3$, $\lambda_{2k+1}^{\mathbf{ABC}} = \lambda_{2k+2}^{\mathbf{ABC}}$.
- $x \mapsto \lambda_1(\dot{\Omega}_{X(x)}^{\mathcal{R}})$ and $x \mapsto \lambda_1(\dot{\Omega}_{\check{X}(x)}^{\mathcal{R}})$ equal $\lambda_1(\Omega)$, in adequation with the theoretical result (3.1).
- $x \mapsto \lambda_2(\dot{\Omega}_{X(x)}^{\mathcal{R}}) = \lambda_1^{\mathbf{AB}X(x)}$ and $x \mapsto \lambda_2(\dot{\Omega}_{\check{X}(x)}^{\mathcal{R}}) = \lambda_1^{\mathbf{AB}\check{X}(x)}$ are strictly increasing from $[0, \frac{1}{2}]$ onto $[\lambda_1(\Omega), \lambda_1^{\mathbf{ABC}}]$ and the eigenfunctions are symmetric. The equality between $\lambda_2(\dot{\Omega}_{\check{X}}^{\mathcal{R}})$ and $\lambda_1^{\mathbf{AB}X}$ was proved in (3.1).
- $x \mapsto \lambda_3(\dot{\Omega}_{X(x)}^{\mathcal{R}}) = \lambda_2^{\mathbf{AB}X(x)}$ and $x \mapsto \lambda_3(\dot{\Omega}_{\check{X}(x)}^{\mathcal{R}}) = \lambda_2^{\mathbf{AB}\check{X}(x)}$ are strictly decreasing from $[0, \frac{1}{2}]$ onto $[\lambda_2^{\mathbf{ABC}}, \lambda_2(\Omega)]$ and the eigenfunctions are antisymmetric. The equality between $\lambda_3(\dot{\Omega}_{\check{X}}^{\mathcal{R}})$ and $\lambda_2^{\mathbf{AB}X}$ was proved in (3.1).
- $\lambda_4(\dot{\Omega}_{\check{X}}^{\mathcal{R}}) = \lambda_5(\dot{\Omega}_{\check{X}}^{\mathcal{R}}) = \lambda_2(\Omega)$, for $X = X(x)$ or $X = \check{X}(x)$. This numerical observation is more accurate than the theoretical result deduced from (3.2): $\lambda_4(\dot{\Omega}_{\check{X}}^{\mathcal{R}}) \leq \lambda_2(\Omega)$. This relation seems to be an equality for any X , see Subsection 4.2.
- $x \mapsto \lambda_6(\dot{\Omega}_{X(x)}^{\mathcal{R}}) = \lambda_3^{\mathbf{AB}X(x)}$ and $x \mapsto \lambda_6(\dot{\Omega}_{\check{X}(x)}^{\mathcal{R}}) = \lambda_3^{\mathbf{AB}\check{X}(x)}$ are strictly increasing from $[0, \frac{1}{2}]$ onto $[\lambda_3(\Omega), \lambda_3^{\mathbf{ABC}}]$ and the eigenfunctions are symmetric.

Once the symmetry is admitted, the monotonicity results directly of a domain monotonicity.

Let us now discuss properties specific to each symmetry.

Spectral variation for poles along the axis $y = \frac{1}{2}$.

We observe that when $X(x) = (x, \frac{1}{2})$, $x \mapsto \lambda_k^{\mathbf{AB}X(x)}$ is monotonically increasing for $k = 1, 3, 5$, whereas it is decreasing for $k = 2, 4$.

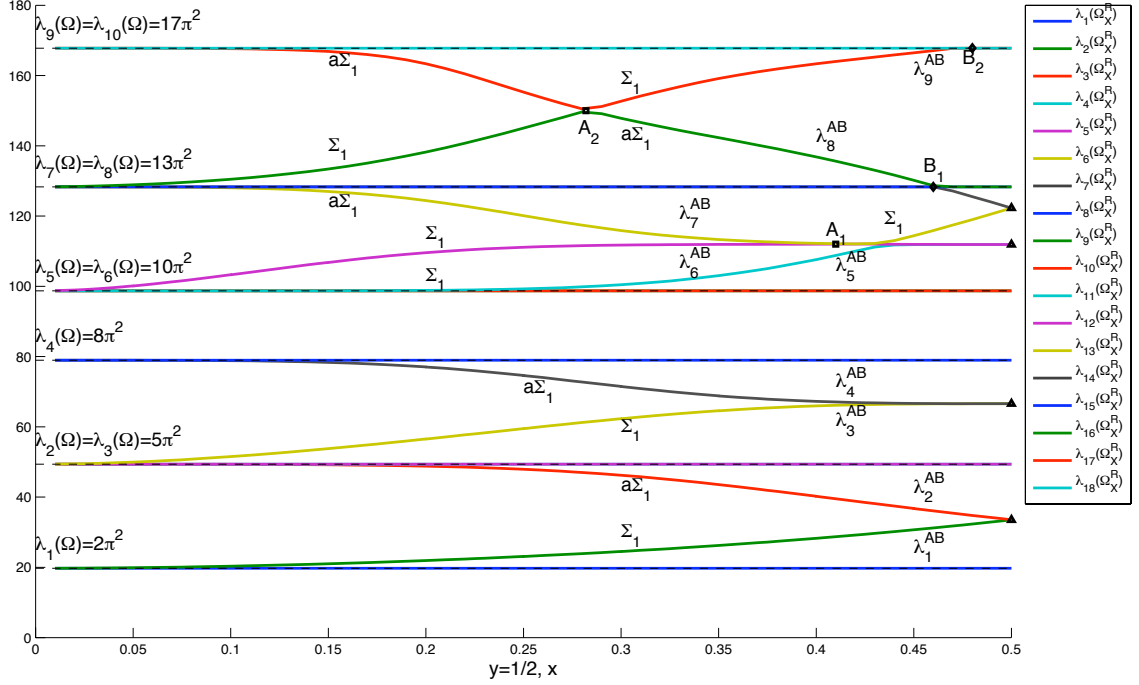


Figure 11: Moving the pole along the axis $y = 1/2$.

We introduce $A_j = X(a_j)$, $B_j = X(b_j)$ specific points which can be seen on Figure 11. We observe numerically:

- (h₁) $x \mapsto \lambda_7(\dot{\Omega}_{X(x)}^{\mathcal{R}}) = \lambda_4^{\mathbf{AB}X(x)}$ is strictly decreasing from $[0, \frac{1}{2}]$ onto $[\lambda_4^{\mathbf{ABC}}, \lambda_4(\Omega)]$ and the eigenfunctions are antisymmetric.
- (i₁) $\lambda_8(\dot{\Omega}_{X(x)}^{\mathcal{R}}) = \lambda_4(\Omega)$. We have proved in (3.8) that $\lambda_8(\dot{\Omega}_{X(x)}^{\mathcal{R}}) \leq \lambda_4(\Omega)$ and we observe that this upper bound is actually an equality. We notice that there is a gap between $\lambda_4(\Omega)$ and $\lambda_5(\Omega)$ where there is no eigenvalue $\lambda_k(\dot{\Omega}_{X(x)}^{\mathcal{R}})$ for X on the perpendicular bisector. This observation is no more true for poles on the diagonal (see Figure 12).
- (j₁) $\lambda_9(\dot{\Omega}_{X(x)}^{\mathcal{R}}) = \lambda_{10}(\dot{\Omega}_{X(x)}^{\mathcal{R}}) = \lambda_5(\Omega)$.
- (k₁) $x \mapsto \lambda_{11}(\dot{\Omega}_{X(x)}^{\mathcal{R}}) = \lambda_5^{\mathbf{AB}X(x)}$ is strictly increasing from $[0, \frac{1}{2}]$ onto $[\lambda_5(\Omega), \lambda_5^{\mathbf{ABC}}]$ and the eigenfunctions are symmetric. This observation shows that the theoretical upper bound $\lambda_{11}(\dot{\Omega}_{X(x)}^{\mathcal{R}}) \leq \lambda_7(\Omega)$ deduced from (3.5) can not be improved.
- (l₁) $x \mapsto \lambda_{12}(\dot{\Omega}_{X(x)}^{\mathcal{R}}) = \lambda_6^{\mathbf{AB}X(x)}$ is strictly increasing from $[0, a_1]$ onto $[\lambda_6(\Omega), \lambda_6^{\mathbf{ABA}_1}]$ and the eigenfunctions are symmetric. It is strictly decreasing from $[a_1, \frac{1}{2}]$ onto $[\lambda_6^{\mathbf{ABC}}, \lambda_6^{\mathbf{ABA}_1}]$ and the eigenfunctions are antisymmetric. This illustrates theoretical result deduced from (3.9): $\lambda_{12}(\dot{\Omega}_{X(x)}^{\mathcal{R}}) \leq \lambda_7(\Omega)$ and shows that this result is optimal.

- (m₁) $x \mapsto \lambda_{13}(\dot{\Omega}_X^{\mathcal{R}}(x)) = \lambda_7^{\mathbf{AB}X(x)}$ is strictly decreasing from $[0, a_1]$ onto $[\lambda_7(\Omega), \lambda_7^{\mathbf{AB}A_1}]$ and the eigenfunctions are antisymmetric. It is strictly increasing from $[a_1, \frac{1}{2}]$ onto $[\lambda_7^{\mathbf{ABC}}, \lambda_7^{\mathbf{AB}A_1}]$ and the eigenfunctions are symmetric. We observe then that $\lambda_{13}(\dot{\Omega}_X^{\mathcal{R}})$ can be bounded from above by $\lambda_7(\Omega)$ whereas we have proved in (3.6) the upper bound by $\lambda_9(\Omega)$.
- (n₁) $\lambda_{14}(\dot{\Omega}_X^{\mathcal{R}}(x))$ equals $\lambda_8(\Omega)$ on $[0, b_1]$. It equals $\lambda_8^{\mathbf{AB}X(x)}$ on $[b_1, \frac{1}{2}]$ and is strictly decreasing from $[b_1, \frac{1}{2}]$ onto $[\lambda_8^{\mathbf{ABC}}, \lambda_8(\Omega)]$ with antisymmetric eigenfunctions.
- (o₁) $\lambda_{15}(\dot{\Omega}_X^{\mathcal{R}}(x)) = \lambda_8(\Omega)$.

Spectral variation for poles along the axis $y = x$.

Figure 12 gives the eigenvalues for poles along the diagonal line of the square $x = y$ with $0 < x \leq 1/2$.

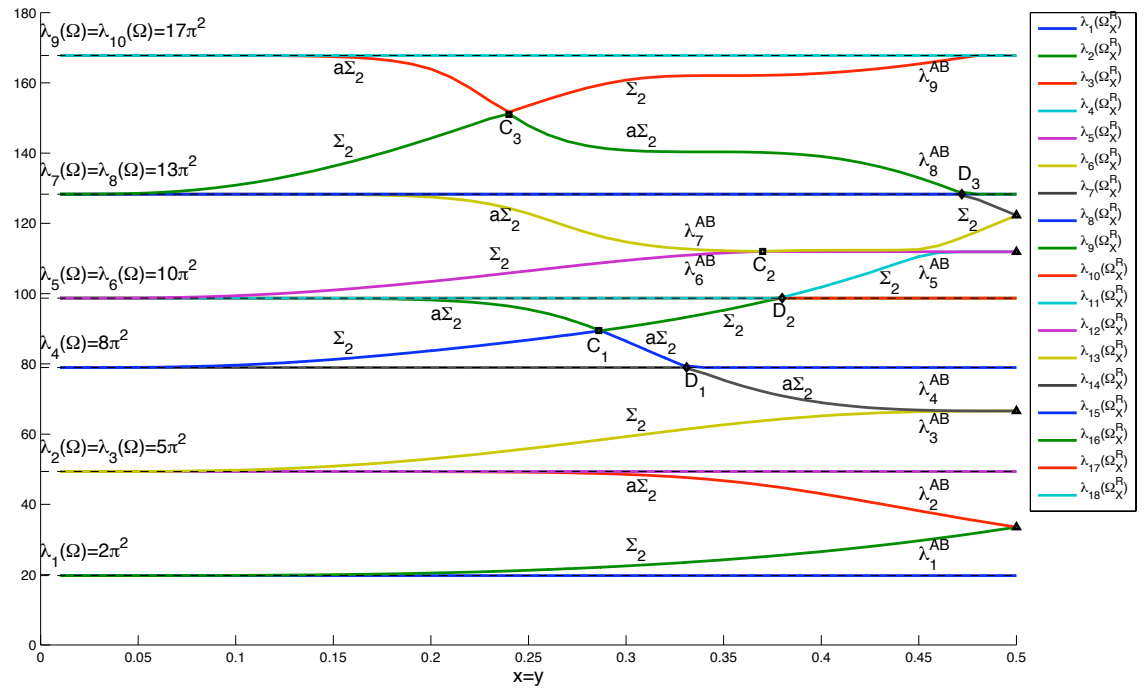


Figure 12: Moving the poles on the diagonal.

We introduce $C_j = \check{X}(c_j)$, $D_j = \check{X}(d_j)$ specific crossing points appearing on the figure. Then, we observe:

- (h₂) $x \mapsto \lambda_7(\dot{\Omega}_X^{\mathcal{R}}(x))$ equals $\lambda_4(\Omega)$ on $[0, d_1]$ and $\lambda_4^{\mathbf{AB}\check{X}(x)}$ on $[d_1, \frac{1}{2}]$ where it is strictly decreasing onto $[\lambda_4^{\mathbf{ABC}}, \lambda_4(\Omega)]$ and the eigenfunctions are antisymmetric. This numerical computations show that the theoretical estimate $\lambda_7(\dot{\Omega}_X^{\mathcal{R}}) \leq \lambda_4(\Omega)$, deduced from (3.3) is optimal.
- (i₂) $\lambda_8(\dot{\Omega}_X^{\mathcal{R}}(x))$ equals $\lambda_4^{\mathbf{AB}\check{X}(x)}$ on $[0, d_1]$ and $\lambda_4(\Omega)$ on $[d_1, \frac{1}{2}]$. It is strictly increasing from $[0, c_1]$ onto $[\lambda_4(\Omega), \lambda_4(\dot{\Omega}_{C_1}^{\mathcal{R}})]$ with symmetric eigenfunctions and strictly decreasing from $[c_1, d_1]$ onto $[\lambda_4(\Omega), \lambda_4(\dot{\Omega}_{C_1}^{\mathcal{R}})]$ with antisymmetric eigenfunctions. This illustrates that (3.4) is optimal.

- (j₂) $\lambda_9(\dot{\Omega}_{\tilde{X}(x)}^{\mathcal{R}})$ equals $\lambda_5^{\mathbf{AB}\tilde{X}(x)}$ on $[0, d_2]$ and $\lambda_5(\Omega)$ on $[d_2, \frac{1}{2}]$. It is strictly decreasing from $[0, c_1]$ onto $[\lambda_4(\dot{\Omega}_{C_1}^{\mathcal{R}}), \lambda_5(\Omega)]$ with antisymmetric eigenfunctions and strictly increasing from $[c_1, d_1]$ onto $[\lambda_4(\dot{\Omega}_{C_1}^{\mathcal{R}}), \lambda_5(\Omega)]$ with symmetric eigenfunctions.
- (k₂) $\lambda_{10}(\dot{\Omega}_{\tilde{X}(x)}^{\mathcal{R}}) = \lambda_5(\Omega)$.
- (l₂) $x \mapsto \lambda_{11}(\dot{\Omega}_{\tilde{X}(x)}^{\mathcal{R}})$ equals $\lambda_5(\Omega)$ on $[0, d_2]$ and $\lambda_5^{\mathbf{AB}\tilde{X}(x)}$ on $[d_2, \frac{1}{2}]$ where it is strictly increasing onto $[\lambda_5(\Omega), \lambda_5^{\mathbf{ABC}}]$ and the eigenfunctions are symmetric. This illustrates the fact that relation (3.5) is optimal.
- (m₂) $x \mapsto \lambda_{12}(\dot{\Omega}_{\tilde{X}(x)}^{\mathcal{R}}) = \lambda_6^{\mathbf{AB}\tilde{X}(x)}$ is strictly increasing from $[0, c_2]$ onto $[\lambda_6(\Omega), \lambda_6^{\mathbf{ABC}_2}]$ and the eigenfunctions are symmetric. It is strictly decreasing from $[c_2, \frac{1}{2}]$ onto $[\lambda_6^{\mathbf{ABC}}, \lambda_6^{\mathbf{ABC}_2}]$ and the eigenfunctions are antisymmetric.
- (n₂) $x \mapsto \lambda_{13}(\dot{\Omega}_{\tilde{X}(x)}^{\mathcal{R}}) = \lambda_7^{\mathbf{AB}\tilde{X}(x)}$ is strictly decreasing from $[0, c_2]$ onto $[\lambda_7(\Omega), \lambda_7^{\mathbf{ABC}_2}]$ and the eigenfunctions are antisymmetric. It is strictly increasing from $[c_2, \frac{1}{2}]$ onto $[\lambda_7^{\mathbf{ABC}}, \lambda_7^{\mathbf{ABC}_2}]$ and the eigenfunctions are symmetric. We then observe $\lambda_{13}(\dot{\Omega}_{\tilde{X}(x)}^{\mathcal{R}}) \leq \lambda_7(\Omega)$ whereas we have proved the weaker upper bound by $\lambda_9(\Omega)$ in (3.6).
- (o₂) $\lambda_{14}(\dot{\Omega}_{\tilde{X}(x)}^{\mathcal{R}})$ equals $\lambda_7(\Omega)$ on $[0, d_3]$. It equals $\lambda_8^{\mathbf{AB}\tilde{X}(x)}$ on $[d_3, \frac{1}{2}]$ and is strictly decreasing from $[d_3, \frac{1}{2}]$ onto $[\lambda_8^{\mathbf{ABC}}, \lambda_8(\Omega)]$ with antisymmetric eigenfunctions.
- (p₂) $\lambda_{15}(\dot{\Omega}_{\tilde{X}(x)}^{\mathcal{R}}) = \lambda_8(\Omega)$.

5.3 Exchange of symmetry and crossing points

When moving the pole on one bisector or one diagonal, and for each eigenvalue of multiplicity 1, the corresponding K_X -real eigenfunction should be either symmetric or antisymmetric with respect to Σ_j^c . Figure 11 suggests that there exist two poles $A_1 = (a_1, \frac{1}{2})$ and $A_2 = (a_2, \frac{1}{2})$ on the perpendicular bisector such that $\lambda_{12}(\dot{\Omega}_{A_1}^{\mathcal{R}})$ and $\lambda_{16}(\dot{\Omega}_{A_2}^{\mathcal{R}})$ are eigenvalues of multiplicity 2. Taking the Aharonov-Bohm point of view, this corresponds to a crossing between $\lambda_6^{\mathbf{AB}\tilde{X}(x)}$ and $\lambda_7^{\mathbf{AB}\tilde{X}(x)}$ for $x = a_1$, with $a_1 \in]\frac{42}{100}, \frac{43}{100}[$ and to a crossing between $\lambda_8^{\mathbf{AB}\tilde{X}(x)}$ and $\lambda_9^{\mathbf{AB}\tilde{X}(x)}$ at $x = a_2$, with $a_2 \in]\frac{28}{100}, \frac{29}{100}[$. The nodal sets of the corresponding eigenfunctions are given in Figure 13. The first line gives the eigenvalues $\lambda_6^{\mathbf{AB}\tilde{X}}, \lambda_8^{\mathbf{AB}\tilde{X}}$ and the associated nodal sets, and the second line $\lambda_7^{\mathbf{AB}\tilde{X}}, \lambda_9^{\mathbf{AB}\tilde{X}}$ and the corresponding nodal set for X along the perpendicular bisector and close to A_1, A_2 .

Figure 12 suggests that there are 3 points, C_1, C_2 and C_3 on the diagonal such that $\lambda_8(\dot{\Omega}_{C_1}^{\mathcal{R}}), \lambda_{12}(\dot{\Omega}_{C_2}^{\mathcal{R}})$ and $\lambda_{16}(\dot{\Omega}_{C_3}^{\mathcal{R}})$ are eigenvalues of multiplicity 2. This corresponds to a crossing between $\lambda_4^{\mathbf{AB}\tilde{X}(x)}$ and $\lambda_5^{\mathbf{AB}\tilde{X}(x)}$ at $x = c_1$, with $c_1 \in]\frac{28}{100}, \frac{29}{100}[$. Similarly, there is a crossing between $\lambda_6^{\mathbf{AB}\tilde{X}(x)}$ and $\lambda_7^{\mathbf{AB}\tilde{X}(x)}$ at $x = c_2$, with $c_2 \in]\frac{36}{100}, \frac{37}{100}[$, and also between $\lambda_8^{\mathbf{AB}\tilde{X}(x)}$ and $\lambda_9^{\mathbf{AB}\tilde{X}(x)}$ at $x = c_3$, with $c_3 \in]\frac{23}{100}, \frac{24}{100}[$. The nodal set of the corresponding eigenfunctions are given in Figures 14.

Looking at Figures 13 and 14, we can verify that there exists an exchange of symmetry³ predicting the existence of the points A_j and C_j .

³Look at the horizontal or diagonal nodal line joining the pole to the boundary!

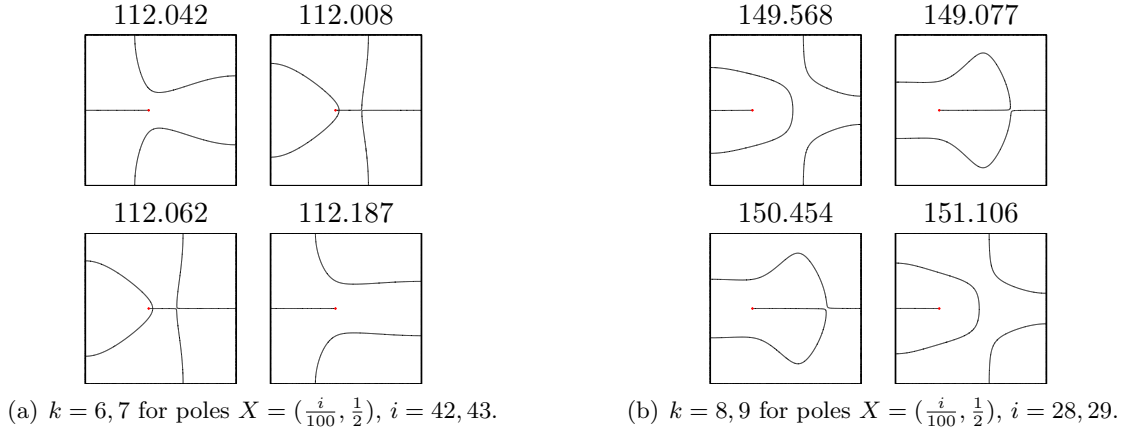


Figure 13: Change of symmetry on the nodal sets associated with $\lambda_k^{\mathbf{AB}X(x)}$.

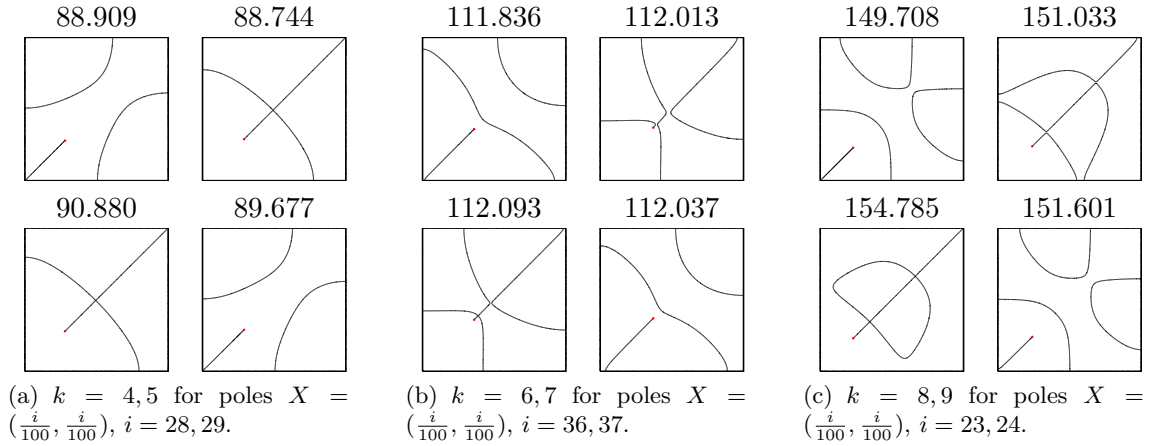


Figure 14: Nodal set for the eigenfunctions associated with $\lambda_k^{\mathbf{AB}X}$

5.4 Nodal deformation: an example

Figure 15 gives the deformation mechanism for the nodal set associated with the fifth eigenvalue of the $\mathbf{AB}X$ -Hamiltonian for poles $X = (\frac{i}{100}, \frac{1}{2})$, $1 \leq i \leq 50$, on the perpendicular bisector of one side of the square. Between the fourth and fifth subfigures, we have a nodal structure where there are two double points at the boundary.

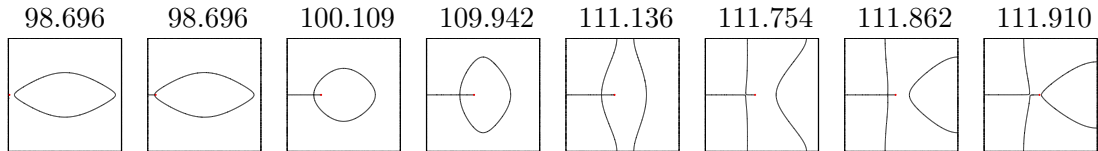


Figure 15: Nodal set for the 5-th eigenfunction of the \mathbf{AB} -Hamiltonian with poles $X = (\frac{i}{100}, \frac{1}{2})$, $i = 1, 7, 30, 42, 43, 44, 45, 49$.

5.5 Moving the pole without respecting the symmetries of the square

Figure 16 gives the eigenvalues $\lambda_k(\dot{\Omega}_X^{\mathcal{R}})$ for $1 \leq k \leq 12$ when the pole X belongs to the line $y = \frac{1}{4} + \frac{x}{2}$. We choose this axis to exhibit a case without symmetry and we notice that the **AB**-eigenvalues $\lambda_k^{\mathbf{AB}X}$ are no longer monotone with respect to x when $X = (x, \frac{1}{4} + \frac{x}{2})$. The result should be the same for any arbitrary line (except the perpendicular bisector and the diagonal). We choose to present the simulations for this line because this line contains enough points in \mathcal{P} to use the previous numerical computations.

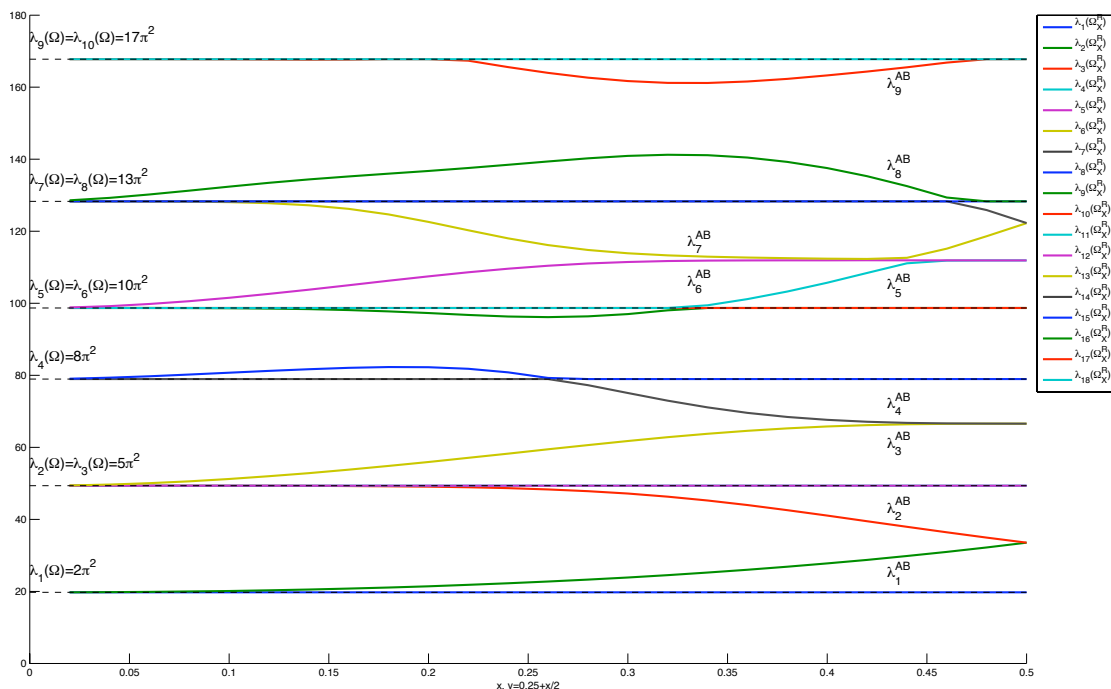


Figure 16: Moving the pole along the axis $y = \frac{1}{4} + \frac{x}{2}$, $0 \leq x \leq \frac{1}{2}$.

It would be interesting to make computations for a finer grid of $X = (x, \frac{1}{4} + \frac{x}{2})$ for x around 0.44 to detect possible crossings between $\lambda_5^{\mathbf{AB}X}$, $\lambda_6^{\mathbf{AB}X}$ and $\lambda_7^{\mathbf{AB}X}$.

6 Nodal sets and minimal partitions

The analysis of $\lambda_5^{\mathbf{AB}X}$ and $\lambda_6^{\mathbf{AB}X}$ leads us to guess numerically the existence of a double eigenvalue when X is the center. As for the pairs $\lambda_3^{\mathbf{AB}X}$ and $\lambda_4^{\mathbf{AB}X}$ which lead us to the family of candidates for the minimal 3-partitions of the square (see Subsection 4.3), we are led to produce a candidate for a minimal 5-partition for the square, with the property that it is minimal inside the class of 5-partitions which can be lifted to $\dot{\Omega}_C^{\mathcal{R}}$. Although $\lambda_5^{\mathbf{ABC}} = \lambda_{11}(\dot{\Omega}_C^{\mathcal{R}})$ is not Courant-sharp⁴ for the Dirichlet Laplacian on $\dot{\Omega}_C^{\mathcal{R}}$, we observe that it is Courant-sharp for the **ABC**-Hamiltonian.

This time, neither numerics nor theory is giving the existence of a continuous family of 5-partitions. Actually, one knows from elementary results on the perturbation of harmonic polynomials of order 2 that the perpendicular crossing of two lines will generically disappear by perturbation.

⁴The index is 11 and not 10.

In the unit ball of the 2-dimensional eigenspace of $\lambda_{11}(\dot{\Omega}_C^{\mathcal{R}})$ we only find four eigenfunctions leading to four distinct configurations whose projection on one sheet has five domains. These eigenfunctions are symmetric or antisymmetric with respect to one of the four bisectors of the square (see Figure 17). The other configurations seem to have (see below) four symmetric (for the deck map) pairs of domains. Looking at the linear combination $tu_{11} + (1-t)u_{12}$ of the eigenfunction associated with $\lambda_{11}(\dot{\Omega}_C^{\mathcal{R}})$ and $\lambda_{12}(\dot{\Omega}_C^{\mathcal{R}})$, we observe in Figure 17 that the triple point is very unstable and only appears for $t \simeq \frac{96}{200}$ and $t \simeq \frac{194}{200}$ when we consider $0 \leq t \leq 1$.

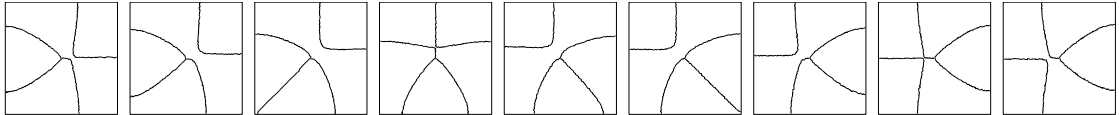


Figure 17: Nodal sets of the linear combination of u_{11} and u_{12} with $t = \frac{1}{200}(0, 25, 55, 96, 125, 138, 175, 194, 200)$.

Of course it is interesting to compare with what can be obtained by looking at other topological types for the minimal 5-partitions. We recall that these types can be classified by using Euler formula (see [13] for the case of 3-partitions). Inspired by [11], we look for a partition which has the symmetries of the square and four critical points. We get two types of models and using the symmetries, we can reduce to a Dirichlet-Neumann problem on a triangle corresponding to the eighth of the square (see Figure 18 where we impose Neumann conditions on dashed lines). Moving the Neumann boundary on one side like in



Figure 18: Dirichlet-Neumann problem on the eighth of the square.

[5] leads to two candidates. Numerical computations demonstrate a lower energy in one case which coincides with one of the pictures in [11] (see Figure 19).

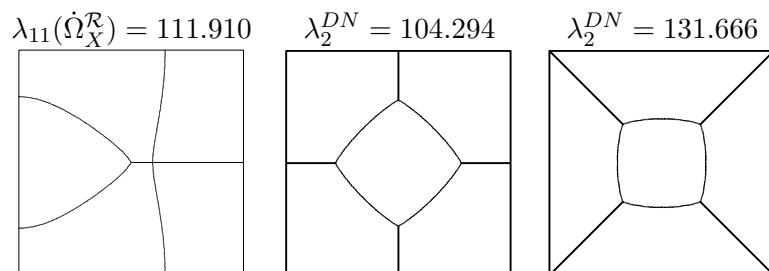


Figure 19: Three candidates for the 5-partition of the square.

Remark 6.1

Note that in the case of the disk a similar analysis leads to a different answer. The

partition of the disk by five halfrays with equal angle has a lower energy than the minimal 5-partition with four singular points (see Figure 20). We note that, on the basis of standard computations (see for example (A1) and (A5) in [14], Appendix A) this energy corresponds to the eleventh eigenvalue of the Dirichlet problem on the double covering on the punctured disk (hence is not Courant-sharp) but corresponds to the fifth eigenvalue of the Aharonov-Bohm spectrum on the punctured disk at the center. Hence it is Courant-sharp in the sense developed in [15] (for the sphere) and it shows the minimality of this 5-partition inside the class of the 5-partitions of the disk having a unique critical point which is, in addition, at the center.

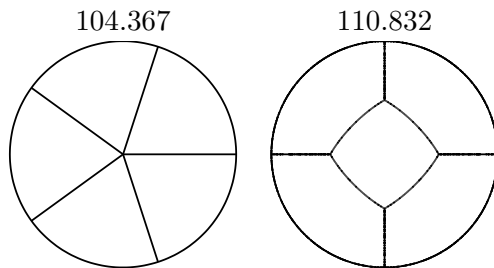


Figure 20: Two candidates for the 5-partition of the disk.

7 Conclusion

We have explored rather systematically how minimal partitions could be obtained by looking at nodal domains of a problem on the double covering of a punctured square. We have analyzed the behavior of the nodal set when moving the pole in the square. This has permitted to confirm the status of “main” candidate for some 3-partitions in the case of the square. This has also permitted to exhibit a natural candidate for a minimal 5-partition which finally appears to be less favorable than another partition with four critical points. This is a starting point for a program which can be developed in at least two directions:

- analyze other domains,
- do the same work by considering the double covering of a multi-punctured domain and moving the poles.

This program is related to the following conjecture

Conjecture 7.1 *Let Ω be a simply connected open set of \mathbb{R}^2 ,*

$$\mathfrak{L}_k(\Omega) = \inf_{\ell \in \mathbb{N}} \inf_{X_1, \dots, X_\ell} L_k^{\mathbf{AB}}(\dot{\Omega}_{X_1, \dots, X_\ell}).$$

Here, for ℓ distinct points $\mathbf{X} = (X_1, \dots, X_\ell)$ in Ω , $L_k^{\mathbf{AB}}(\Omega_{X_1, \dots, X_\ell})$ is defined as follows. First we can extend our construction of an Aharonov-Bohm Hamiltonian in the case of a configuration with ℓ points (putting a (renormalized) flux $\frac{1}{2}$ at each of these points). We can also construct (see [12]) the antilinear operator $K_{\mathbf{X}}$ and consider the $K_{\mathbf{X}}$ -real eigenfunctions. $L_k^{\mathbf{AB}}(\dot{\Omega}_{X_1, \dots, X_\ell})$ denotes the smallest eigenvalue of the $\mathbf{AB} - (X_1, \dots, X_\ell)$ Hamiltonian for which there is an eigenfunction with k -nodal domains.

Let us present a few examples to illustrate the conjecture. When $k = 2$, there is no need to consider punctured Ω 's. The infimum is obtained for $\ell = 0$. When $k = 3$, it is possible

to show that it is enough, to minimize over $\ell = 0$, $\ell = 1$ and $\ell = 2$. In the case of the disk and the square, it is proven that the infimum cannot be for $\ell = 0$ and we conjecture that the infimum is for $\ell = 1$ and attained for the punctured domain at the center. For $k = 5$, in the case of the square, it seems that the infimum is for $\ell = 4$ and for $\ell = 1$ in the case of the disk.

Let us explain very briefly why this conjecture is natural. Considering a minimal k -partition, we denote by X_1, \dots, X_ℓ the critical points of the partition corresponding to an odd number of meeting half-lines. Then we suspect that $\mathfrak{L}_k(\Omega) = \lambda_k^{\mathbf{AB}}(\dot{\Omega}_{X_1, \dots, X_\ell})$ (Courant-sharp situation). Conversely, any family of nodal domains of an Aharonov-Bohm operator on $\dot{\Omega}_{X_1, \dots, X_\ell}$ corresponding to $L_k^{\mathbf{AB}}$ gives a k -partition. Using the Euler formula, see [13], we obtain easily that the maximal number of critical points with an odd number of meeting half-lines ℓ is bounded from above by $2k - 3$.

In other words, when the minimal partition is not nodal, we conjecture that it is actually the projection of a nodal partition of suitable eigenfunction on the double covering for a suitable puncturing \mathbf{X} .

References

- [1] B. ALZIARY, J. FLECKINGER-PELLÉ, P. TAKÁČ. Eigenfunctions and Hardy inequalities for a magnetic Schrödinger operator in \mathbb{R}^2 . *Math. Methods Appl. Sci.* **26**(13) (2003) 1093–1136.
- [2] J. BERGER, J. RUBINSTEIN. On the zero set of the wave function in superconductivity. *Comm. Math. Phys.* **202**(3) (1999) 621–628.
- [3] V. BONNAILLIE-NOËL, B. HELFFER. Numerical analysis of nodal sets for eigenvalues of Aharonov-Bohm Hamiltonians on the square and application to minimal partitions. *Preprint ESI* **2193** (2009).
- [4] V. BONNAILLIE-NOËL, B. HELFFER, T. HOFFMANN-OSTENHOF. Aharonov-bohm Hamiltonians, isospectrality and minimal partitions. *J. Phys. A: Math. Theor.* **42**(18) (2009) 185203, 20pp.
- [5] V. BONNAILLIE-NOËL, B. HELFFER, G. VIAL. Numerical simulations for nodal domains and spectral minimal partitions. *ESAIM Control Optim. Calc. Var.* **16**(1) (2010) 221–246.
- [6] V. BONNAILLIE-NOËL, G. VIAL. Computations for nodal domains and spectral minimal partitions.
<http://w3.bretagne.ens-cachan.fr/math/simulations/MinimalPartitions>
(2007).
- [7] F. BOZORGNIA. Numerical algorithm for spatial segregation of competitive systems. *SIAM J. Scientific Computing* **31**(5) (2009) 3946–3958.
- [8] M. CONTI, S. TERRACINI, G. VERZINI. An optimal partition problem related to nonlinear eigenvalues. *J. Funct. Anal.* **198**(1) (2003) 160–196.
- [9] M. CONTI, S. TERRACINI, G. VERZINI. On a class of optimal partition problems related to the Fučík spectrum and to the monotonicity formulae. *Calc. Var. Partial Differential Equations* **22**(1) (2005) 45–72.

- [10] M. CONTI, S. TERRACINI, G. VERZINI. A variational problem for the spatial segregation of reaction-diffusion systems. *Indiana Univ. Math. J.* **54**(3) (2005) 779–815.
- [11] O. CYBULSKI, V. BABIN, R. HOŁYST. Minimization of the Renyi entropy production in the space-partitioning process. *Phys. Rev. E (3)* **71**(4) (2005) 046130, 10.
- [12] B. HELFFER, M. HOFFMANN-OSTENHOF, T. HOFFMANN-OSTENHOF, M. P. OWEN. Nodal sets for groundstates of Schrödinger operators with zero magnetic field in non-simply connected domains. *Comm. Math. Phys.* **202**(3) (1999) 629–649.
- [13] B. HELFFER, T. HOFFMANN-OSTENHOF. On spectral minimal partitions: new properties and applications to the disk. *To appear in Proceedings of the conference in Montreal. CRM Lectures* (2009).
- [14] B. HELFFER, T. HOFFMANN-OSTENHOF, S. TERRACINI. Nodal domains and spectral minimal partitions. *Ann. Inst. H. Poincaré Anal. Non Linéaire* **26** (2009) 101–138.
- [15] B. HELFFER, T. HOFFMANN-OSTENHOF, S. TERRACINI. On spectral minimal partitions: the case of the sphere. *Around the Research of Vladimir Maz'ya III, International Math. Series* **13** (2010) 153–178.
- [16] L. HILLAIRET, C. JUDGE. The eigenvalues of the Laplacian on domains with small slits. *arXiv : 0802.2597*. To appear in *Trans. AMS* (2009).
- [17] D. JAKOBSON, M. LEVITIN, N. NADIRASHVILI, I. POLTEROVICH. Spectral problems with mixed Dirichlet-Neumann boundary conditions: isospectrality and beyond. *J. Comput. Appl. Math.* **194**(1) (2006) 141–155.
- [18] M. LEVITIN, L. PARNOVSKI, I. POLTEROVICH. Isospectral domains with mixed boundary conditions. *J. Phys. A* **39**(9) (2006) 2073–2082.
- [19] D. MARTIN. MÉLINA, bibliothèque de calculs éléments finis.
<http://perso.univ-rennes1.fr/daniel.martin/melina> (2007).
- [20] B. NORIS, S. TERRACINI. Nodal sets of magnetic Schrödinger operators of Aharonov–Bohm type and energy minimizing partitions. *Preprint* (2009).
- [21] B. NORIS, S. TERRACINI. In preparation (2009).
- [22] J. R. SHEWCHUK. Triangle: A two-dimensional quality mesh generator and Delaunay triangulator.
<http://www.cs.cmu.edu/~quake/triangle.html> (2005).